Wind and Structures, *Vol. 33, No. 2 (2021) 115-122*
https://doi.org/10.12989/was.2021.33.2.115

Generating unconventional wind flow in an actively controlled multi-fan wind tunnel

Wei Cui[1,2a], Lin Zhao*[1,2,3], Shuyang Cao[1,2b] and Yaojun Ge[1,2c]

[1]*State Key Lab of Disaster Reduction in Civil Engineering, Tongji University, Shanghai 200092, China*
[2]*Key Laboratory of Transport Industry of Wind Resistant Technology for Bridge Structures, Tongji University, Shanghai 200092, China*
[3]*State Key Laboratory of Mountain Bridge and Tunnel Engineering, Chongqing Jiaotong University, Chongqing 400074, China*

(*Received March 1, 2021, Revised July 13, 2021, Accepted August 3, 2021*)

Abstract. In this study, an iteration-based method to simulate two typical examples of unconventional wind flow in a multi-fan wind tunnel is described: skewed non-Gaussian turbulence and sinusoidal type transient gust. The air flows are generated by 120 actively controlled fans arranged in a 10 wide by 12 high matrix. Time-varying voltages signals can be imported into the fans' servomotors, then corresponding wind flow can be produced in this wind tunnel. At first, the target wind speeds time series are converted to voltages signals, which are input into the fans' motor next, and then the initial wind flow generated can be measured. Then the wind speeds time series to be input are adjusted according to the differences between the target winds speeds and measured flow speeds. The above procedure is iteratively repeated until the measured wind flow is gradually close to the targets. At last, both non-Gaussian turbulence and transient gust can be simulated with satisfied precision after several iterations.

Keywords: actively controlled multi-fan wind tunnel; iteration; Non-Gaussian Turbulence; transient gust

1. Introduction

Recently, an actively controlled multi-fan wind tunnel has been developed in State Key Lab of Disaster Reduction in Civil Engineering of Tongji University, mainly for the purpose of reproducing the complex turbulence wind field with transient and non-Gaussian features for wind engineering applications.

Pioneeringly, Cao *et al*. (2001) developed a 2-D actively controlled wind tunnel equipped with multi-fan airfoils for reproducing the various wind field in the atmospheric boundary layer (ABL) for engineering applications. Each fan installed in this wind tunnel is controlled by computers individually. Through the controlled movement of fans and airfoils, it is able to generate a range of steady or fluctuating flows. At first, it presents an iteration-based algorithm to generate the von Kàrmàn type turbulence, which presents the full power spectral density (PSD) for a very wide frequency band. Afterward, utilizing the multiple arrays of fans, the wind field of ABL is reproduced in the wind tunnel, including several key features: Reynolds stress coefficient, turbulence intensity, turbulence integral length, and vertical wind profile. Later, a 3-D actively controlled multi-fan wind tunnel is developed by the same wind engineering team to generate the non-stationary intermittent turbulence time history and the down-burst transient wind field (Cao *et al*. 2002). In the above two wind tunnels, regular turbulence with Gaussian distribution and vertical wind profile in atmospheric boundary layer are successfully generated based iteration principle.

In recent years, the research about turbulence has been extended from conventional Gaussian turbulence to unconventional wind field (Solari *et al*. 2015). Meanwhile, as the development of high frequency wind speed monitoring equipment, an increasing number of studies about wind turbulence characteristics during typhoon emphasizing on transient and non-Gaussianity has been reported (Quan *et al*. 2020). Yin *et al*. (2016) pointed out that the turbulence non-Gaussianity will become more obvious as the turbulence scale decrease and propose to use wavelet based method to simulate non-Gaussian turbulence. In a recent study, Zhao *et al*. (2019) reported a unified model about turbulence characteristics from the four measured typhoon records, which shows turbulence distribution, especially when near typhoon center, has positive skewness and non-Gaussian characteristics. The higher-order properties of typhoon wind turbulence distribution have not been the main concern in most previous studies (Cao *et al*. 2009).

Meanwhile, the transient gust is another recent research topic for wind engineering field. Several research on wind climate environment have argued that the wind speeds are rapidly varying, which originates from non-synoptic wind climate such as thunderstorms, downburst storms (Darwish *et al*. 2010, Aboshosha and El Damatty 2015), hurricanes (Wang *et al*. 2016, Tao *et al*. 2020) and tornadoes (Cao *et al*. 2019, Le and Caracoglia 2019). Therefore, the

*Corresponding author, Professor
E-mail: zhaolin@tongji.com
[a]Ph.D. Assistant Professor
E-mail: cuiwei@tongji.edu.cn
[b]Ph.D. Professor
E-mail: shuyang@tongji.edu.cn
[c]Ph.D. Professor
E-mail: yaojunge@tongji.edu.cn

ISSN: 1226-6116 (Print), 1598-6225 (Online)

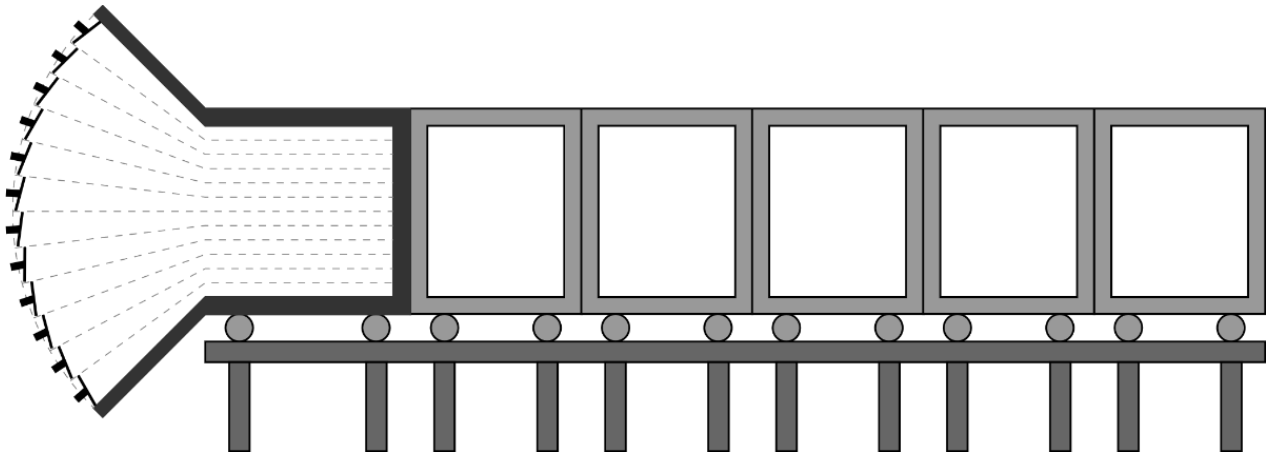

Fig. 1 Schematic sectional view of the 3-D multi-fan wind tunnel in Tongji University

simulation of transient wind field physically in wind tunnel is essential to investigate the dynamic response of slender large span (Ibrahim *et al*. 2020).

With the help of the actively controlled multi-fan wind tunnel, it is possible to produce the two unconventional wind climates: skewed non-Gaussian turbulence and transient gust. This kind of wind speeds cannot be generated in traditional wind tunnel, where turbulence is generated by ground roughness blocks and spires. Because of adjustable rotation speeds of fans, the time-varying and non-Gaussian wind flow is possible to be produced. This study will extend the iteration method proposed in Cao *et al*. (2001), which was used to simulate conventional wind field, to generate unconventional wind flow through two examples in actively controlled multi-fan wind tunnel, which will be used to study the bluff-body aerodynamics in this non-conventional wind environment (Hao and Wu 2018).

2. The 3-D multi-fan wind tunnel and measurement setup in Tongji University

Fig. 1 shows the schematic of the 3-D wind tunnel section. This wind tunnel is an open-circuit one with 120 fans of 270 mm in diameter, which are arranged in a 12 (vertical) by 10 (wide) matrix. The test section is 1500~mm wide, and 1800~mm high. In the along-wind direction, the wind tunnel wall has been modular separated, thus the length of the test section and location of testing model can be adjusted. Each fan is driven by AC servo-motors through individual computer. The servomotors can be controlled at different frequencies of up to 20 Hz, through which fluctuating flow is achieved in the wind tunnel. Fig. 2 is the photo of 12 × 10 fan array. In this study, the generated wind field is measured at 5 m downstream from the fans array (Cao *et al*. 2009), by a group of two Cobra probe three-directional anemometers. One anemometer is located at the middle of wind tunnel height (0.9 m), and another one as the backup is located at the three-quarter height (1.35 m). The photos taken from wind tunnel outlet and lateral sides are shown in Figs. 3(a) and 3(b). The default duration of the measuring sampling frequency of 62.5 Hz, which will keep the same through this study.

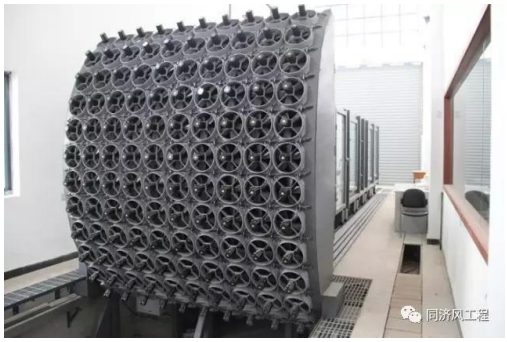

Fig. 2 The fan array of multi-fan wind tunnel in Tongji University

3. Case one: Non-Gaussian turbulence

Previous measured typhoon turbulence records, especially near the typhoon center, has positive skewness. Fig. 4 shows two turbulence examples and related probabilistic distribution with different skewness from the outer region of typhoon Bolaven (2012) measured at Xihoumen Bridge's site, and Fig. 4 clearly shows that the histogram deviated from fitted Gaussian function. Li *et al*. (2019) also shows that typhoon wind field contains high gust in large turbulence intensity situation. However, the positive skewed high gust as shown in Fig. 4 cannot be modeled using Gaussian process.

The higher-order properties of typhoon wind turbulence distribution have not been the main concern in most previous studies. Cao *et al*. (2009) states that skewness and kurtosis are independent of wind speeds. Li *et al*. (2015) showed that skewness and kurtosis have a weak correlation with turbulence intensity. However, in conventional boundary layer, only Gaussian turbulence can be generated through grid or ground roughness blocks. Thus, it is necessary to develop the new procedure to produce non-Gaussian turbulence in multi-fan wind tunnel.

3.1 Numerically simulating the time series of non-Gaussian turbulence

According to the Shinozuka equation in Eq. (1), the

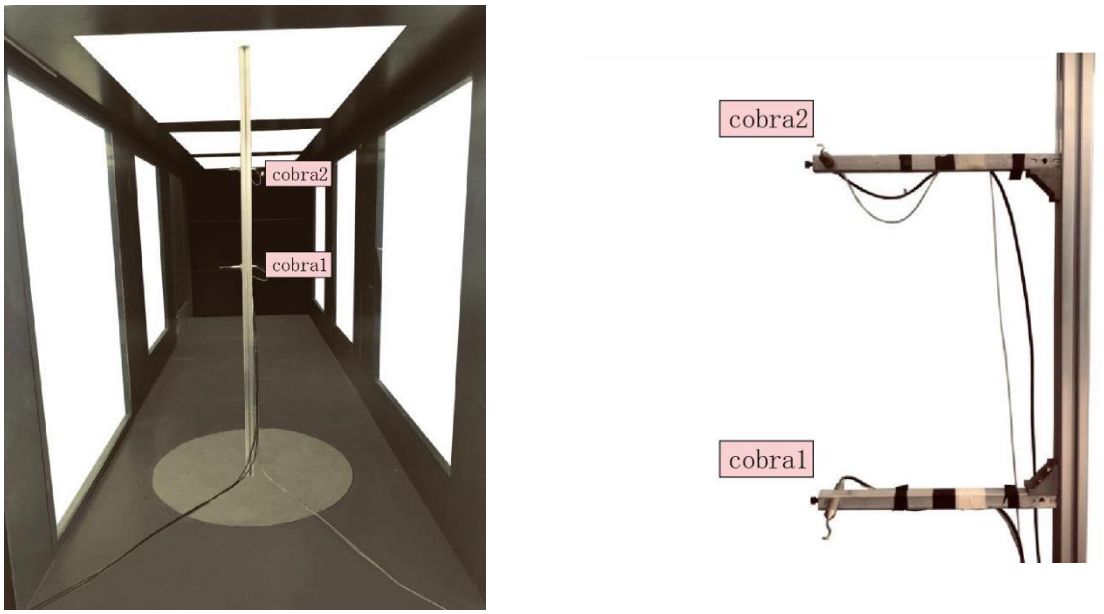

(a) View from wind tunnel outlet (b) Lateral view

Fig. 3 Arrangement of two cobra anemometers in multi-fan wind tunnel

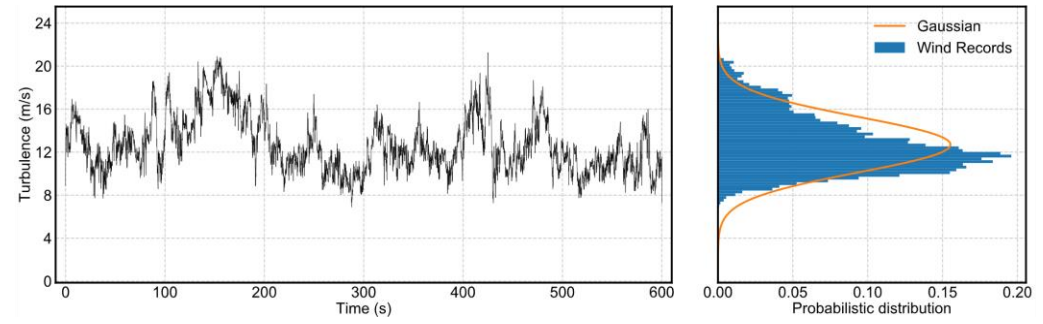

(a) skewness ≈ 1

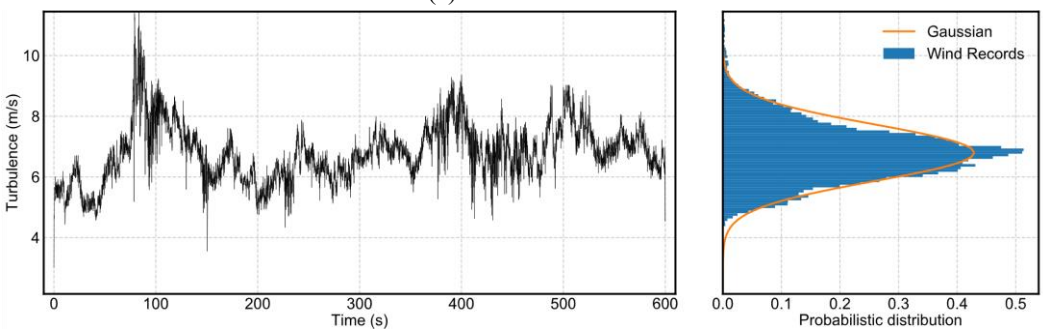

(b) skewness ≈ 0.5

Fig. 4 Examples of positive skewed turbulence from typhoon Bolaven (2012)

Gaussian turbulence time series $u_i(t)$ at multiple sequential points can be generated using spectral representation method. Meanwhile, the non-Gaussian turbulence is simulated by the translation process established by Grigoriu (1984) to ensure the consistency of the turbulence spectrum as well as the turbulence intensity.

$$u_i(t) = \sqrt{4\pi\Delta n}\sum_{m=1}^{i}\sum_{l=1}^{N}|H_{im}(n_{ml})|\cos(2\pi n_{ml}t - \theta_{im}(n_{ml}) + \Phi_{ml}) \quad (1)$$

where N is the number of evaluated frequency points, which is should be sufficiently large. $\Delta n = \frac{n_{\mathrm{up}}}{N}$ is the frequency increment, and n_{up} is the upper cutoff frequency. Φ_{ml} is the independent random phone angles. $H_{im}(n_{ml})$ is derived from Cholesky's decomposition of the required turbulence PSD S_{uu} and θ_{im} is the complex angle of H_{im}.

The von Kàrmàn spectrum shown in Eq. (2) is employed in this study as the target turbulence spectrum to be simulated in the multi-fan wind tunnel.

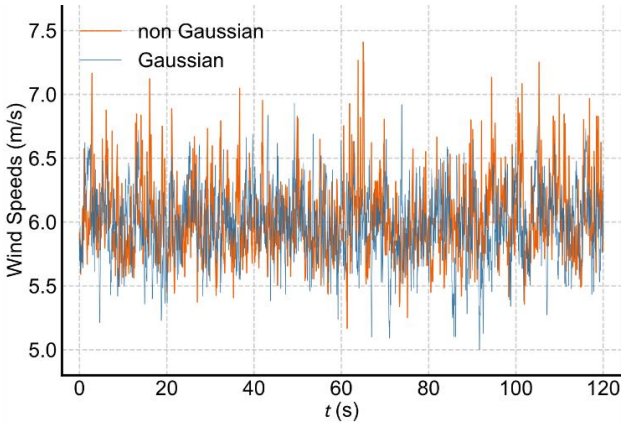

(a) Time Domain

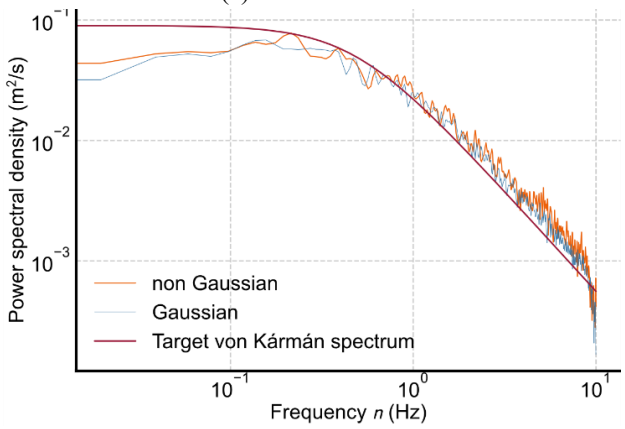

(b) Frequency Domain

Fig. 5 Numerical simulated Gaussian and non-Gaussian turbulence sample

$$\frac{nS_{uu}}{\sigma_u^2} = \frac{4\frac{nL_u}{U}}{\left[1+70.8\left(\frac{nL_u}{U}\right)^2\right]^{\frac{5}{6}}} \tag{2}$$

where σ_u is the standard deviation of the turbulence u, U is the mean wind speed and L_u is the turbulence integral length. σ_u is normally normalized to wind speed U, and expressed as turbulence intensity $I_u = \frac{\sigma_u}{U}$.

Figs. 5(a) and Fig. 5(b) illustrates 120s time series of numerical generated Gaussian and non-Gaussian turbulence with skewness $\gamma = 1$, respectively. The dependence of kurtosis κ on skewness γ is assumed to follow the relationship found in Zhao *et al*. (2019) and shown in Eq. (3).

$$\kappa_u = 2.862\gamma_u^2 + 3 \tag{3}$$

For comparison purposes, the random phase angel Φ_{ml} in Eq. (1) is the same for Gaussian and non-Gaussian turbulence. The non-Gaussian turbulence sample illustration in demonstrates the positive skewed distribution, while the turbulence spectrum features with different skewness are identical, which is demonstrated in Fig. 5(b). It should be noted that the turbulence shown in Fig. 5 are generated directly in model scale (lab scale) and does not present full scale turbulence presented in Fig. 4.

3.2 The method of reproducing non-Gaussian turbulent wind in multi-fan wind tunnel

For the actively controlled fans, the generated wind velocity is linearly dependent on voltage signal, which is directly related to the fan rotational speeds. The method of reproducing the skewed non-Gaussian turbulent wind velocity history has two major steps:

- Generating Gaussian turbulence containing sufficient energy component (PSD) for required frequency range;
- Adjust input wind speeds time series through Hermite polynomial transfer function to required skewness and kurtosis.

At the beginning, for illustration purpose, one set of turbulence parameters is simulated in wind tunnel and retested in this study, whose mean velocity, turbulent intensity, integral scale, skewness and kurtosis are U=6 m/s, I_u =5%, L_u =1.5m, γ_u =0.75 and γ_u =4.61$, respectively.

3.2.1 Generating Gaussian turbulence

The Gaussian turbulence generation procedure is detailed presented in Cao *et al*. (2002). At first, signal of target turbulence is input into the fans' motors. However, turbulent flow needs travel certain distance until reaching measuring location, the PSD for higher frequency will decay faster than the turbulence at lower turbulence range. Thus, an iteration method was proposed in Cao *et al*. (2002) to adjust the input signal which has higher PSD, so that the turbulence after decay can approximately reach the target PSD. The iteration formula is:

$$S_{uu}^{k+1,i}(n) = S_{uu}^{k,i}(n)\frac{S_{uu}^{t}(n)}{S_{uu}^{k,m}(n)} \tag{4}$$

in which $S_{uu}^{t}(n)$ is target PSD, $S_{uu}^{k,i}(n)$ is the PSD of input signal for fans' motors for iteration k and $S_{uu}^{k,m}(n)$ is the measured turbulence PSD for iteration k. It should be noted that, in the original methods proposed in Cao *et al*. (2002), the turbulence phase can also be adjusted.

Fig. 6 shows the time series and PSD in frequency domain of generated turbulence after three iterations. It is clear that, for the 1st iteration, the measured PSD has large discrepancy comparing with target PSD, especially for high frequency range. However, after 5 iterations the PSD of measured turbulence has increased to the target level for $n < 3$ Hz. Because of the output torque configured in servo-motors, there is a limitation of servo-motors reciprocating rotation maneuverability. Therefore, the turbulence PSD larger for $n > 3$ Hz cannot be achieved in this wind tunnel. Regardless the input voltage signal magnitude, the PSD of measured wind speed remain at very low level.

3.2.2 Generating skewed non-Gaussian turbulence

The servo-motors input signal for skewed turbulence can be calculate through Hermite transfer function in Yang and Gurley (2015). Similar to turbulence PSD, the skewness also decays along the wind flow traveling from fans to flow measuring sensor. Therefore, a same iterative procedure is applied to approximately reach the turbulence skewness:

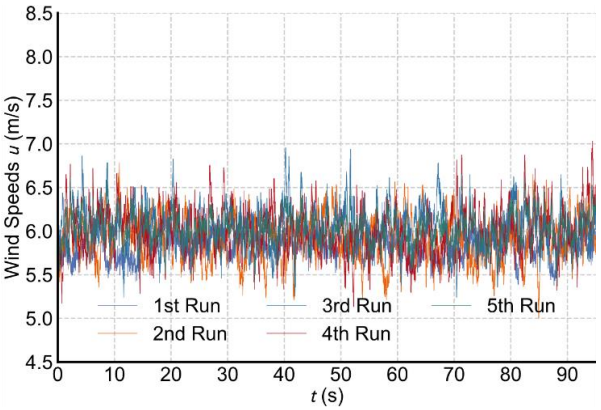

(a) Time Domain

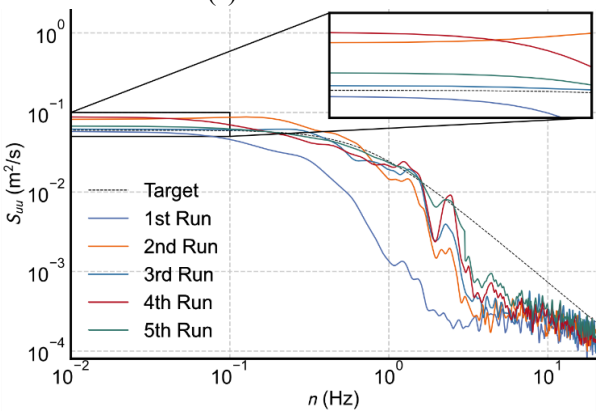

(b) Frequency Domain

Fig. 6 Iteration method for generating Gaussian turbulence

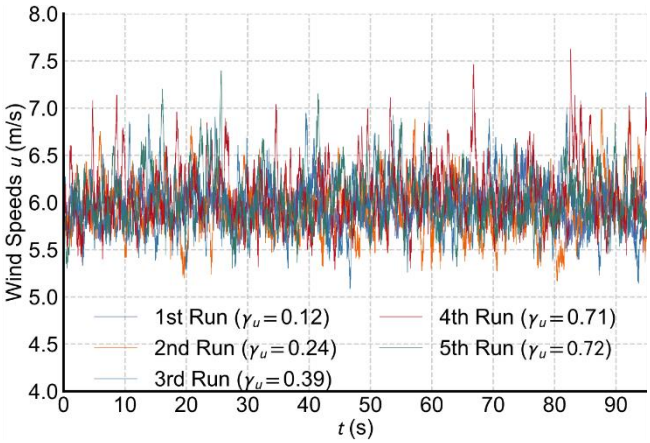

(a) Time Domain

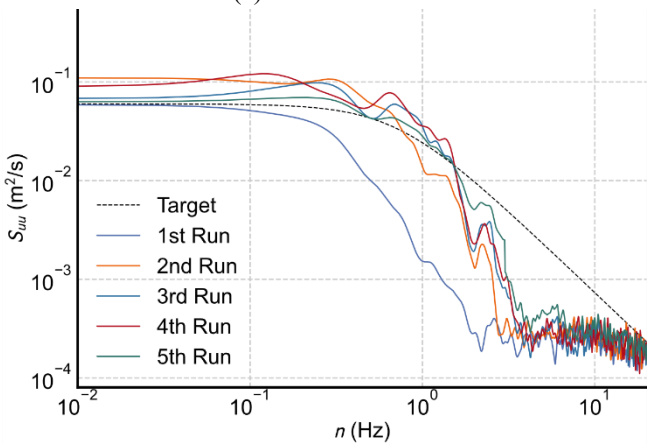

(b) Frequency Domain

Fig. 7 Iteration method for generating non-Gaussian turbulence

$$\gamma_{uu}^{k+1,i} = \gamma_{uu}^{k,i} \frac{\gamma_{uu}^{t}}{\gamma_{uu}^{k,m}} \tag{5a}$$

$$S_{uu}^{k+1,i}(n) = S_{uu}^{k,i}(n) \frac{S_{uu}^{t}(n)}{S_{uu}^{k,m}(n)} \tag{5b}$$

In the above iteration, γ is the signal skewness and the superscripts keep the same meaning as Eq. (4)

Fig. 7 shows that the generated turbulence can sustain the required PSD as previous step, and also can gradually increase the skewness towards the target skewness.

4. Case two: Sinusoidal type transient gust

The transient gust is another type of unconventional wind flow, which cannot be generated in traditional boundary layer wind tunnel. The transient gust is normally observed in down-burst and tornadoes. In recent studies, sinusoidal type transient gust is employed as a simplified and standardized transient wind flow (Hao and Wu 2017, He *et al*. 2020) to study the aerodynamic and aeroelastic effects on structures. Wu and Kareem (2015) also proposed to use impulse function, which is a generalized version of sinusoidal gust, as the Volterra kernel to simulate the bluff-body nonlinear aerodynamic forces.

The time series of sinusoidal type wind flow can be expressed in the following formula:

$$(t) = A\left[1 + \sin\left(2\pi\frac{t}{T} + \frac{3}{2}\pi\right)\exp(-\lambda t)\right] + v_1 \tag{6}$$

in which A is the wind flow varying amplitude $A = \frac{v_2 - v_1}{2}$, $\exp(-\lambda t)$ is the wind flow adapting function used to smooth the connection between varying stage and stationary stage, λ is the adapting rate $\lambda = -\frac{\ln\left(1-\frac{v_3-v_1}{A}\right)}{T}$, and T is the duration of wind flow varying stage.

Fig. 8 shows a typical implementation of sinusoidal type transient gust with the initial wind speed as v_1, nominal peak wind speed as v_2 and ending wind speed as v_3. It should be noted that, because of the negative exponential decay coefficient $-\lambda$ in adapting function, the nominal peak wind speed v_2 (shown as gray dash line in Fig. 8) is slightly different with actual peak wind speeds.

4.1 The methods of generating sinusoidal type transient gust

Figs. 9-11 shows the wind flows generated from multi-fan wind tunnel with the input signal calculating from Eq. (6) with three different durations: 40 s, 20 s and 10 s. The characteristic wind speeds v_1, v_2, v_3 are 4, 14, 2 m/s, respectively, which are same for gusts in Figs. 9-11. The

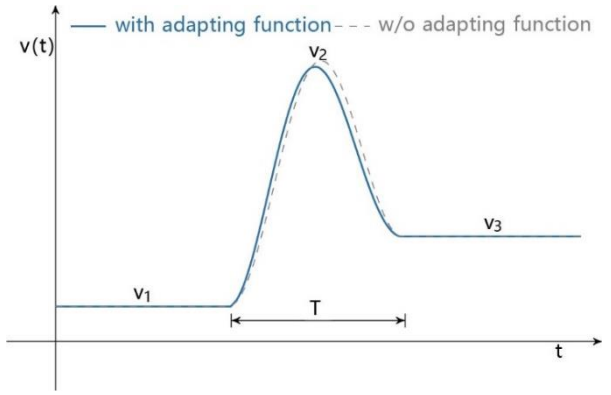

Fig. 8 A typical sinusoidal type transient gust

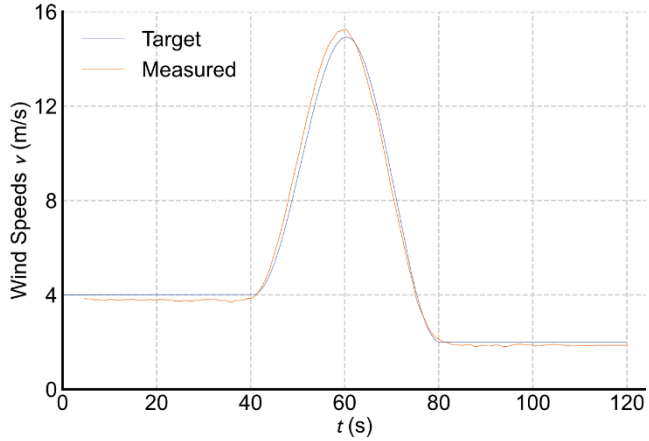

Fig. 9 40s duration of sinusoidal type transient gusts

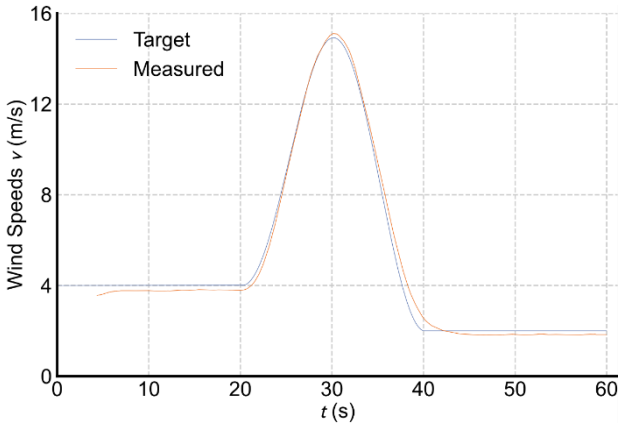

Fig. 10 20 s duration of sinusoidal type transient gusts

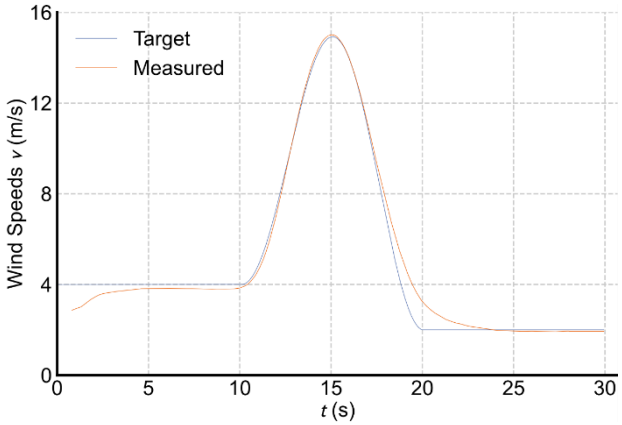

Fig. 11 10 s duration of sinusoidal type transient gusts

measured gust time series are post-processed by a low-pass filter with cut-off frequency at 5Hz and moving average with 1 seconds length window.

For longer duration gust (40s and 20s), the multi-fan wind tunnel can generally produce the designated gust time series. However, for gust with shorter duration (10s), the measured wind flow decreased slower than the required gust time series. When the fan rotating speeds drop very fast according to the designated signal, the air flow at the measuring point with certain distance from fan array cannot response as quickly as the fan array. Therefore, the fan rotating speeds should drop more quickly in advance, so that the measured wind flow can match the required gust time series as closely as possible.

$$v^{k+1,i}(t) = v^{k,i}(t)\left[\frac{v^{d}(t)}{v^{k,m}(t)}\right]^{\alpha} \tag{7}$$

in which k is the iteration number i denotes the input signal, m is the measured wind flow and d means the designated gust time series, α is the adjusting rate within (0, 1]. Figs. 12 and 13 show the iteration steps to generate two sinusoidal type transient gust with same duration (10~s) but different speeds configurations. For the first scenario, the multi-fan wind tunnel can produce the required gust time series after two iterations. In contrast, for the second scenario, because the wind speeds dropping rate is higher, matching the designated gust is more challenging. At the third iteration, the input signal has much lower beforehand decreased wind speeds, the actual wind speeds do not converge obviously towards the designated gust comparing with the second iteration. Thus, the wind speeds dropping rate in second scenario may exceed the capacity of this multi-fan wind tunnel.

5. Conclusions

In this study, an iteration-based measuring-adjusting-feedback method is presented to generate unconventional wind flow in a multi-fan wind tunnel. The traditional boundary layer wind tunnel is only able to produce well-developed turbulence field with stationarity and Gaussian turbulence characters, but unable to generate unconventional wind flow, such as skewed non-Gaussian turbulence and transient short-duration gust. However, because in multi-fan wind tunnel, certain distance is required between fan array and model test location, the measured flow and input signal to fan motor are different due to turbulence decaying and diffusion. Therefore, in this study, the difference between target wind flow and measured results are employed as calibrating ratio to adjust the input signal for next steps. Employing this iteration principle, the multi-fan wind tunnel can produce the non-Gaussian turbulence and short duration transient gust with required turbulence characteristics and sinusoidally varying gust.

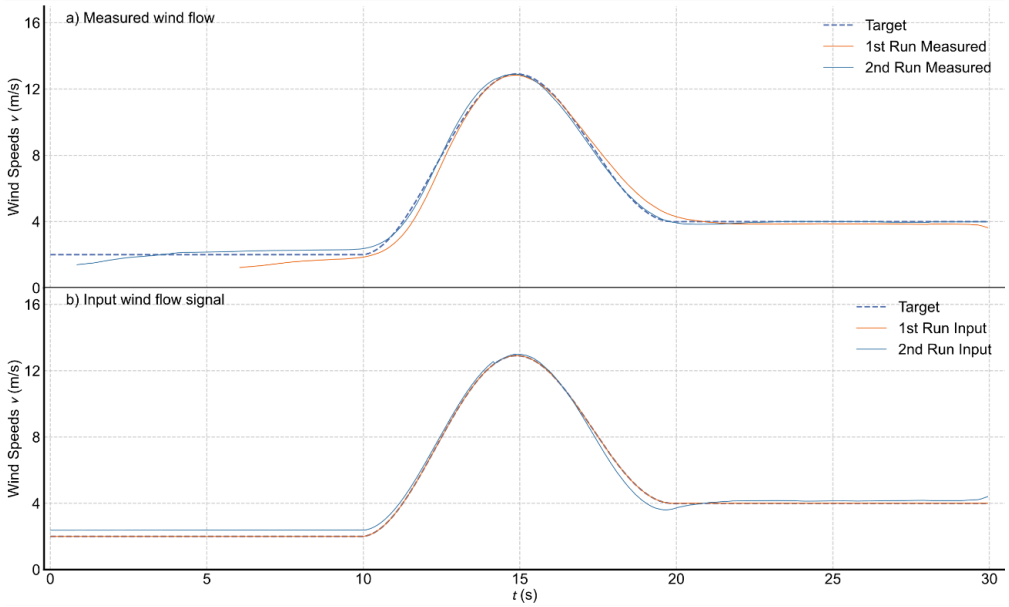

Fig. 12 Simulated sinusoidal type transient gust with 10s duration and $v_1 = 2, v_2 = 14,\ v_3 = 4$ m/s

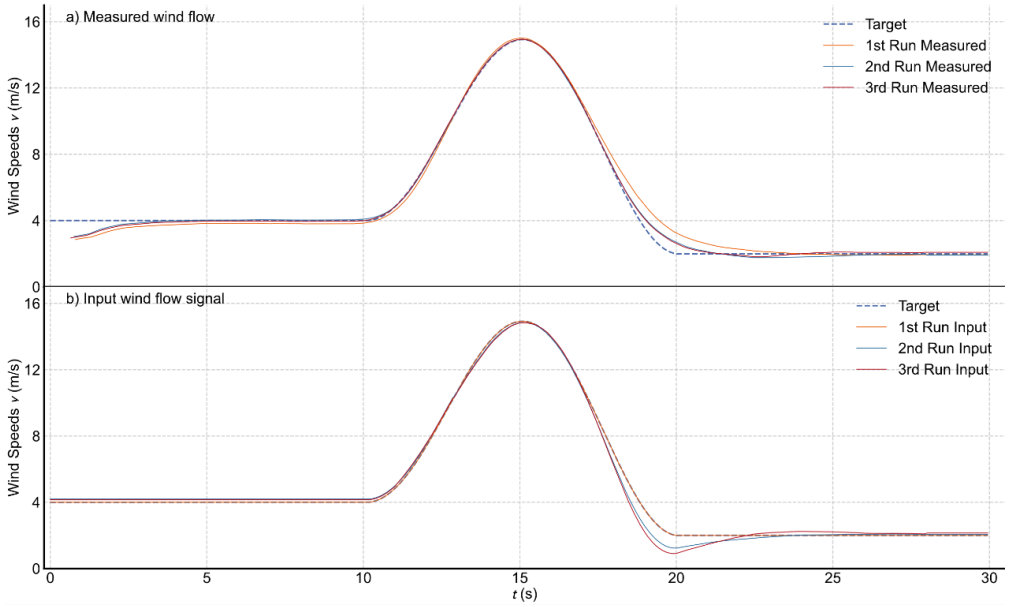

Fig. 13 Simulated sinusoidal type transient gust with 10s duration and $v_1 = 4, v_2 = 14,\ v_3 = 2$ m/s

Acknowledgments

The authors gratefully acknowledge the support of National Natural Science Foundation of China (52008314, 52078383) and Shanghai Pujiang Program (No. 19PJ1409800). Any opinions, findings and conclusions or recommendations are those of the authors and do not necessarily reflect the views of the above agencies.

References

Aboshosha, H. and El Damatty, A. (2015), "Dynamic response of transmission line conductors under downburst and synoptic winds", *Wind Struct*., **21**(2), 241-272. https://dx.doi.org/10.12989/was.2015.21.2.241.

Cao, J., Ren, S., Cao, S. and Ge, Y. (2019), "Physical simulations on wind loading characteristics of streamlined bridge decks under tornado-like vortices", *J. Wind Eng. Ind. Aerod*., **189**, 56-70. https://doi.org/10.1016/j.jweia.2019.03.019.

Cao, S., Nishi, A., Hirano, K., Ozono, S., Miyagi, H., Kikugawa, H., Matsuda, Y. and Wakasugi, Y. (2001), "An actively controlled wind tunnel and its application to the reproduction of the atmospheric boundary layer", *Bound. Lay. Meteorol*., **101**(1), 61-76. https://doi.org/10.1023/A:1019288828837.

Cao, S., Nishi, A., Kikugawa, H. and Matsuda, Y. (2002), "Reproduction of wind velocity history in a multiple fan wind tunnel", *J. Wind Eng. Ind. Aerod*., **90**(12), 1719-1729. https://doi.org/10.1016/S0167-6105(02)00282-9.

Cao, S., Tamura, Y., Kikuchi, N., Saito, M., Nakayama, I. and Matsuzaki, Y. (2009), "Wind characteristics of a strong typhoon", *J. Wind Eng. Ind. Aerod*., **97**(1), 11-21. https://doi.org/10.1016/j.jweia.2008.10.002.

Darwish, M.M., El Damatty, A.A. and Hangan, H. (2010), "Dynamic characteristics of transmission line conductors and behaviour under turbulent downburst loading", *Wind Struct.*, **13**(**4**), 327-346. https://doi.org/10.12989/was.2010.13.4.327.

Grigoriu, M. (1984), "Crossings of non-Gaussian translation processes", *J. Eng. Mech. (ASCE)*, **110**(4), 610-620. https://doi.org/10.1061/(ASCE)0733-9399(1984)110:4(610).

Hao, J. and Wu, T. (2017), "Nonsynoptic wind-induced transient effects on linear bridge aerodynamics", *J. Eng. Mech.*, **143**(9), 04017092. https://doi.org/10.1061/(ASCE)EM.1943-7889.0001313.

Hao, J. and Wu, T. (2018), "Downburst-induced transient response of a long-span bridge: A CFD-CSD-based hybrid approach", *J. Wind Eng. Ind. Aerod.*, **179**, 273-286. https://doi.org/10.1016/j.jweia.2018.06.006.

He, X.H., Shi, K. and Wu, T. (2020), "An efficient analysis framework for high-speed train-bridge coupled vibration under non-stationary winds", *Struct. Infrastruct. Eng.*, **16**(9), 1326-1346. https://doi.org/10.1080/15732479.2019.1704800.

Ibrahim, I., Aboshosha, H. and El Damatty, A. (2020), "Numerical characterization of downburst wind field at WindEEE dome", *Wind Struct.*, **30**(3), 231-243. https://doi.org/10.12989/was.2020.30.3.231.

Le, V. and Caracoglia, L. (2019), "Generation and characterization of a non-stationary flow field in a small-scale wind tunnel using a multi-blade flow device", *J. Wind Eng. Ind. Aerod.*, **186**, 1-16. https://doi.org/10.1016/j.jweia.2018.12.017.

Li, L., Kareem, A., Xiao, Y., Song, L. and Zhou, C. (2015), "A comparative study of field measurements of the turbulence characteristics of typhoon and hurricane winds", *J. Wind Eng. Ind. Aerod.*, **140**, 49-66. https://doi.org/10.1016/j.jweia.2014.12.008.

Li, L., Zhou, Y., Wang, H., Zhou, H., He, X. and Wu, T. (2019), "An analytical framework for the investigation of tropical cyclone wind characteristics over different measurement conditions", *Appl. Sci.*, **9**(24), 5385. https://doi.org/10.3390/app9245385.

Quan, Y., Fu, G.Q., Huang, Z.F. and Gu, M. (2020), "Comparative analysis of the wind characteristics of three landfall typhoons based on stationary and nonstationary wind models", *Wind Struct.*, **31**(3), 269-285. https://doi.org/10.12989/was.2020.31.3.269.

Solari, G., Burlando, M., De Gaetano, P. and Repetto, M.P. (2015), "Characteristics of thunderstorms relevant to the wind loading of structures", *Wind Struct.*, **20**(6), 763-791. https://doi.org/10.12989/was.2015.20.6.763.

Tao, T.Y., Wang, H., Shi, P. and Li, H. (2020), "Stationary and non-stationary buffeting analyses of a long-span bridge under typhoon winds", *Wind Struct.*, **31**(5), 455-467. https://doi.org/10.12989/was.2020.31.5.455.

Wang, H., Wu, T., Tao, T., Li, A. and Kareem, A. (2016), "Measurements and analysis of non-stationary wind characteristics at Sutong Bridge in Typhoon Damrey", *J. Wind Eng. Ind. Aerod.*, **151**, 100-106. https://doi.org/10.1016/j.jweia.2016.02.001.

Wu, T. and Kareem, A. (2015), "A nonlinear analysis framework for bluff-body aerodynamics: A Volterra representation of the solution of Navier-Stokes equations", *J. Fluids Struct.*, **54**, 479-502. https://doi.org/10.1016/j.jfluidstructs.2014.12.005.

Yang, L. and Gurley, K.R. (2015), "Efficient stationary multivariate non-Gaussian simulation based on a Hermite PDF model", *Probabil. Eng. Mech.*, **42**, 31-41. https://doi.org/10.1016/j.probengmech.2015.09.006.

Yin, C., Wu, T. and Kareem, A. (2016), "Synthetic turbulence: A wavelet based simulation", *Probabil. Eng. Mech.* **45**, 177-187. https://doi.org/10.1016/j.probengmech.2016.05.001.

Zhao, L., Cui, W. and Ge, Y. (2019), "Measurement, modeling and simulation of wind turbulence in typhoon outer region", *J. Wind Eng. Ind. Aerod.*, **195**, 104021. https://doi.org/10.1016/j.jweia.2019.104021.

AD